Proceedings of the Thirty-second (2022) International Ocean and Polar Engineering Conference **www.isope.org**
Shanghai, China, June 5–10, 2022

ISBN 978-1-880653-81-4; ISSN 1098-6189

Inferring optimal hydrodynamic databases for vortex induced cross flow vibration prediction of marine risers using limited sensor measurements.

Andreas Mentzelopoulos [a], José del Águila Ferrandis [a], Dixia Fan [a,b], Samuel Rudy [a], Themistoklis Sapsis [a], Michael S. Triantafyllou [a]
[a] Department of Mechanical Engineering, Massachusetts Institute of Technology, Cambridge, MA, USA
[b] School of Engineering, Westlake University, Hangzhou, Zhejiang, China

ABSTRACT

Accurate prediction of the structural response of flexible cylinder vortex-induced vibrations (VIVs) relies heavily on the accuracy of the acquired hydrodynamic coefficient database. Due to a large number of variables, the construction of systematic hydrodynamic databases from rigid cylinder forced vibration experiments can be time-consuming or even intractable. A novel approach has been implemented in this paper to improve the flexible cylinder VIV prediction by inferring the optimal parametric hydrodynamic database using measurements along with the structure; such a methodology has been demonstrated for uniform straight (flexible) risers in uniform flow using displacement data. This work extends the framework and applies it to the straight riser problem using only limited strain measurements. The predicted amplitude and frequency responses are compared with experimental results.

KEY WORDS: Vortex Induced Vibration; VIV; Marine Risers; Hydrodynamic Database; Optimization; Parametric Database.

INTRODUCTION

Vortex-Induced Vibrations (VIV) have been known to engineers for more than 400 years, first observed by Leonardo da Vinci as "Aeolian Tones," sounds created by vortex-induced pressure fluctuations as the wind passes around obstacles. Extensive studies on the subject have since been conducted (Williamson *et al.*, 2004, Williamson *et al.*, 2008, Bearman *et al.*, 2011, Wu *et al.*, 2012, Wang *et al.*, 2020) , in order to mainly suppress VIV due to their destructive capabilities (Park *et al.*, 2016, Bernitsas *et al.*, 2008, Baek *et al.*, 2009). VIV affect bluff bodies in the presence of currents due to periodic shedding vortices developed in the wake aft bodies. Those vortices lead to an alternating pressure, and if the body is free to move, the pressure variations will synchronize with body motion, creating consistent vibrations. If not dealt with properly, VIV can cause extensive fatigue damage over a prolonged period (Bernitsas *et al.*, 2019). Given the bluff nature of many modern offshore engineering equipment, such as cables, mooring lines, and marine risers (Wu *et al.*, 2017, Fan *et al.*, 2017, Fan *et al.*, 2019), a thorough understanding of the underlying physics of VIV is essential in controlling their effects be they fatigue damage to offshore equipment or energy harnessed from flows (Bernitsas *et al.*, 2008).

Unlike the simple harmonic motion, studies find that VIV can occur across a wide range of oscillating frequencies (Govardhan *et al.*, 2002), known as the "lock-in" range, in which synchronization between vortex shedding and body motion takes place (Williamson *et al.*, 2004, Wang *et al.*, 2020). During "lock-in", moderate response amplitudes occur, typically self-limited to about one diameter. The vortex shedding frequency can differ from the Strouhal frequency of a fixed cylinder because, as work via flow visualization has revealed, the relative motion between the vibrating cylinder and the shed vortices can significantly alter the effective fluid added mass (Wang *et al.*, 2021), resulting in a variable natural frequency as a function of stream velocity (Williamson *et al.*, 1996).

Through experimental (Hover *et al.*, 2001, Raghavan *et al.*, 2011, Xu *et al.*, 2013) and numerical (Evangelinos *et al.*, 2000, Wu *et al.*, 2014, Wang *et al.*, 2021) methods, studies revealed that significant variations of the fluid forces on an oscillating rigid cylinder could occur as a function of the oncoming stream velocity and cylinder motions. These variations are due to changes in the vortex shedding pattern. Therefore, experiments were conducted where a rigid cylinder was forced a prescribed motion in a prescribed flow condition (Sarpkaya *et al.*, 1978). In particular, studies focused on the mean drag coefficient C_d, the lift coefficient in-phase with the velocity C_{lv} and the added mass coefficient in the CF direction C_{my} as functions of the true reduced velocity $V_r = \frac{U}{fd}$ and non-dimensional CF amplitude $\frac{A_y}{d}$, where U is the prescribed fluid velocity; f the prescribed motion frequency; A_y the prescribed motion amplitude; and d the cylinder model diameter (Gopalkrishnan *et al.*, 1993, Sarpkaya *et al.*, 1995, Fan *et al.*, 2019). The experiments showed that regions of positive C_{lv}, denoting net energy transferred from the fluid to structure over one motion period, were located in a certain range of V_r and $\frac{A_y}{d}$. In addition, it was found that the added mass coefficient could vary significantly from negative values to large positive values around the true reduced velocity $V_r = 5.9$. These measured hydrodynamic coefficients resulted in an accurate prediction of the rigid cylinder VIV in the CF direction (Wang *et al.*, 2003), and they have served as databases for fluid forces in semi-empirical flexible riser VIV prediction codes (Roveri *et al.*, 2001, Triantafyllou *et al.*, Zheng et al. *et al.*,2001, 1999, Larsen, 2001).

VIV of flexible bodies is significantly more complex than VIV of rigid bodies. Studies have been conducted to investigate the flow structure interaction of flexible bodies undergoing VIV and revealed very complex behaviors, including various structural modes, responses of traveling waves, and recently multi-modal and multi-frequency vibrations. Insights on the flow past the bodies' wakes, in which boundary layers, shear layers, vortices, and the bodies themselves interact, have been revealed (Fan *et al.*, 2019, Han *et al.*, 2018). Given the flexible nature

of many offshore equipments, the accurate prediction of the flexible cylinder VIV is of great importance to decision-makers in the industry.

Semi-empirical models and prediction programs serve as the current state-of-the-art technologies for VIV prediction. One fundamental assumption these semi-empirical tools employ is strip theory, which they have argued is a valid approximation for the flexible body flow-structure interaction problem (Wang *et al.*, 2021). Among several other parameters, estimation of the hydrodynamic coefficients, such as the added mass coefficient C_{my} as well as the lift coefficient in phase with velocity C_{lv}, is key to the accurate prediction of the body's response. Estimating those coefficients is a nontrivial process that includes performing many forced-vibration experiments with rigid cylinders. Due to the large input parametric space, using brute-force experiments to obtain a general hydrodynamic database suitable for every riser in various conditions is an impossible task.

In this paper, we explore and extend a new paradigm (Rudy *et al.*, 2021) of the hydrodynamic database inference directly from flexible cylinder response: an optimized parametric hydrodynamic database obtained from the comparison between experimental and VIVA(Triantafyllou *et al.*, 1999, Zheng *et al.*, 2011) prediction results which could achieve a significant improvement in the predictive accuracy of the riser structural response. Specifically, we first derive the optimal initial condition for the parametric hydrodynamic database. We then further infer the optimal hydrodynamic database of a straight flexible cylinder in uniform flow using directly measured strain data from limited sensors along the structure.

MATERIALS AND METHODS

Parametrization of the hydrodynamic database

Prior (empirical) information of the approximate shape of the expected added mass coefficient, C_{my} and lift coefficient in phase with velocity, C_{lv}, was used to formulate a set of hydrodynamic parameters. Nineteen parameters (p_i, $i \in [1, 19]$) were selected to describe the C_{my} vs. f_r, $C_{lv,0}$ vs f_r, A_c^* vs f_r, and C_{lv} vs A^* curves which form a complete hydrodynamic coefficient database. Corner points were eliminated using a softplus function; the last parameter (p_{19}) was used as the smoothing factor of the softplus function.

The complete mathematical formulation for the extended nineteen dimensional database parametrization is shown in Appendix I.

Optimization

The goal of the optimization is to infer the hydrodynamic coefficient database, i.e. (C_{my} vs. f_r, $C_{lv,0}$ vs f_r, A_c^* vs f_r, and C_{lv} vs A^* curves) from the experimental observations.

The task of obtaining the hydrodynamic database may be viewed a constrained optimization problem in which the optimal 19-parameters $p_i, i \in [1, 19]$ (each constrained in a specific range) which minimize the discrepancy between forward model prediction and experiments, are searched. The objective function may be defined as the weighted sum of the root mean square error differences between (i) the predicted riser strain and experimentally observed strain and (ii) the predicted riser frequency and the experimentally observed frequency, plus some regularization terms.

Let $\boldsymbol{p}_0$ be the initial set of the 19-parameters defining the hydrodynamic database; running the forward model with $\boldsymbol{p}_0$ (across the range of the experimentally tested velocities) yields an estimate of (i) the riser amplitude across the span(in the cross flow direction) and (ii) the riser frequency for each velocity. The objective function may then be formulated mathematically as follows:

$$J(\boldsymbol{p}) = \sum_{i=1}^{N_{V_r}} \left[\lambda \sqrt{\frac{1}{N} \sum_{n=1}^{N} [\epsilon_{i,n} - \hat{\epsilon}_{i,n}(\boldsymbol{p})]^2} + \sqrt{[f_i - \hat{f}_i(\boldsymbol{p})]^2} \right] + \beta \left[\frac{p_5 - p_1}{0.1} \right]^2 + \gamma |p_{19}|, \tag{1}$$

where N is the number of data points along the riser's span, and N_{V_r} is the number of experiments. The constants λ, β, and γ are chosen arbitrarily. The two regularization terms were added to penalize the distance between p_1 and p_5, and the magnitude of the scaling factor of the softplus function.

Since strain data are readily available from experiments and in practice are much easier to obtain compared to displacement data, it was deemed appropriate to demonstrate that the methodology of inferring the hydrodynamic databases can be successful using strain data to learn hydrodynamic coefficients.

Optimizing this objective function across the 19-dimensional space is nontrivial. A stochastic coordinate descent method is employed to search the space and return the optimal set of hydrodynamic parameters $\boldsymbol{p}$.

RESULT AND DISCUSSION

The nineteen parameter framework was used in conjunction with semi-empirical prediction program VIVA (Triantafyllou *et al.*, 1999, Zheng *et al.*, 2011) in order to infer the optimal hydrodynamic database for the program to predict the amplitude and frequency response of risers. The program was trained with data from experiments conducted as part of the Norwegian Deepwater Programme (NDP) (Braaten *et al.*, 2004). A flexible cylinder with length over diameter ratio $L/D \approx 1400$ was used and the Reynolds numbers tested (based on diameter) were $Re \approx 7.1 \cdot 10^3 - 5.7 \cdot 10^4$. Tested velocities were in the range $0.3 - 2.4$ m/s. The displacement and frequency results for the straight bare riser in uniform flow were used. Although training was done using strain data, the accuracy of the database and forward model was validated against experimental displacement and frequency data (rather than experimental strain data), which were of interest. To avoid any confusion, in this context, the terms riser and flexible cylinder refer to the riser model used in the NDP experiments and are not to be confused with the industry standard "flexible riser" meaning composite pipe.

Initial Condition

Defining a suitable initial condition for the optimization was deemed appropriate since initializing at random would, in the least, slow down the convergence of the optimization algorithm, and possibly be partly carried down to the converged result in regions with not many training points. The physics-informed nominal VIVA (Triantafyllou *et al.*, 1999, Zheng *et al.*, 2011) database which has been obtained via rigid cylinder forced vibrations was selected as the appropriate initial condition.

In order to determine the set of initial parameters $\boldsymbol{p_0}$ which optimally parametrize the VIVA nominal database an optimization problem was formed to minimize the discrepancy between the $C_{lv} = f(A^*, f_r)$ of the

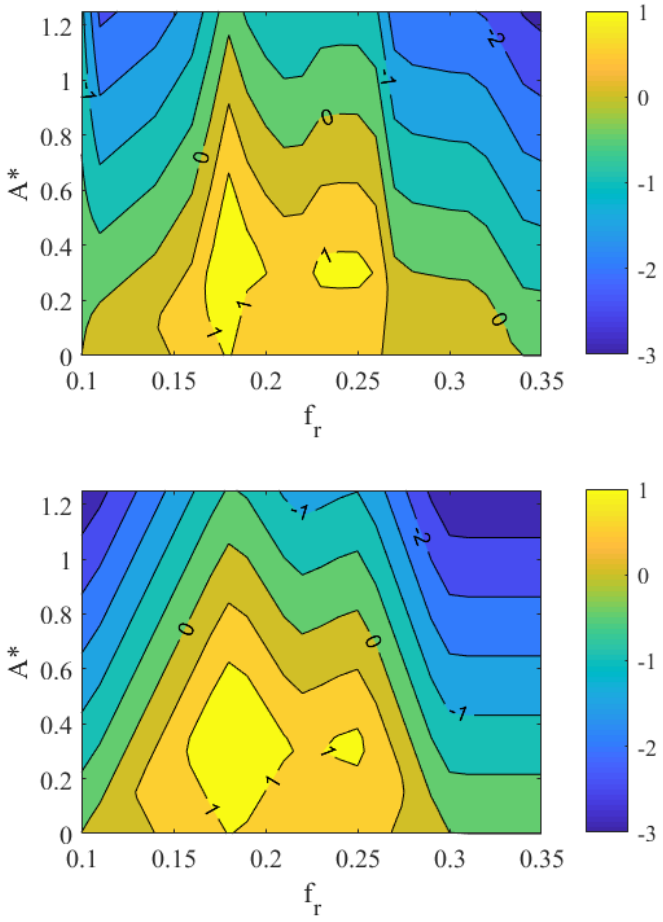

Fig. 1 Gopalkrishnan (1993) lift coefficient contour (top) and parametric database obtained as initial condition (bottom).

nominal VIVA database and the initial parametric database defined by $\hat{C}_{lv} = f(A^*, f_r, \boldsymbol{p_0}), \hat{C}_m = f(f_r, \boldsymbol{p_0})$. The objective function to be minimized in this context may be formulated as follows:

$$J(\boldsymbol{p}) = \sum_{i=1}^{N_{A^*}} \sum_{j=1}^{N_{f_r}} \frac{\sqrt{(C_{lv}(f_{r_j}, A_i^*) - \hat{C}_{lv}(f_{r_j}, A_i^*, \boldsymbol{p}))^2}}{N_{f_{r_j}} \cdot N_{A_i^*}} + \beta |p_{19}|, \tag{2}$$

where N_{f_r} and N_{A^*} are the number of reduced frequencies and number of non-dimensional amplitudes used, respectively. The value of the parameter β was chosen arbitrarily. The resulting C_{lv} contour as well as the training contour are shown in Figure 1.

The optimization was performed accross the range of $f_r = [0.1, 0.35]$ and $A^* = [0, 1.2]$. The reduced order optimized result qualitatively agrees with the training database both in terms of magnitude and contour shape (especially in the $f_r \in [0.15, 0.30]$ range) where most observed VIV responses of moderate amplitude occur. The nineteen (double peak) parametrization offers flexibility in terms of capturing the two "peak" contours of the training database, parametrizing those as piece-wise linear curves.

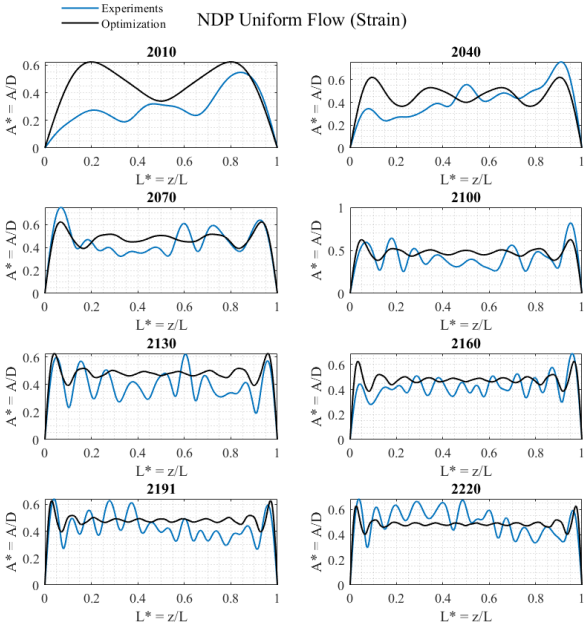

Fig. 2 Amplitude response as a function of span: Non-dimensional amplitude (y-axis) as a function of span (x-axis) is shown for various flow velocities (range: 0.3 - 2.4 m/s). Each subplot (titled with an associated number from NDP experiments) corresponds to a different incoming flow velocity; a higher experiment number corresponds to a higher flow velocity. Experimentally observed (reconstructed) amplitude is shown as a solid blue line while prediction using the optimal hydrodynamic parametric database is shown as a solid black line.

However, the parametrization has limitations as well. For low f_r, close to 0.1 the behavior the Gopalkrishnan contours is not well approximated, as the model is unable to capture the sharp corners of the training set. The same is observed for $f_r > 0.25$, especially for the negative valued contours. Given that VIV occurs at a range of approximately $f_r \in [0.15, 0.30]$ where the parametrization matches the training data closely, the parametric model and initial condition were deemed appropriate, especially since further refinement of the database would follow during the training stage of the optimization.

Optimization using limited strain sensor measurements

Optimization was performed using data from the NDP experiments for a straight riser in uniform flow. Twenty-four uniformly spaced points across the riser's span were used to infer the database where the strain was measured directly (no reconstruction or further data analysis necessary).

In order to determine the accuracy of the inferred databases the displacement prediction as well as the frequency prediction was compared with the reconstructed displacement from experiments as well as the measured frequency for all tested velocities. Indicative amplitude response results are shown in Figure 2 and the frequency response results are shown in Figure 3. The complete amplitude prediction set is included in Appendix II.

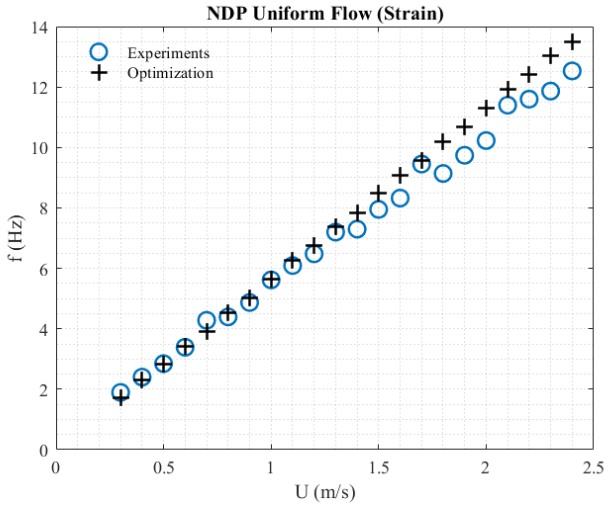

Fig. 3 Frequency response: vibration frequency (y-axis) is plotted against flow velocity (x-axis). Blue circles are the experimentally observed frequencies, and black crosses are the predicted frequencies using the optimal parametric hydrodynamic database.

After training, there is agreement between experimental observation and forward model prediction both in terms of amplitude as a function of span, and in terms of frequency as a function of incoming flow velocity. This result demonstrates how databases need not be inferred from displacement data which are rather expensive to obtain but may be determined directly from limited strain measurements along the structure which are in practice easier to obtain, especially in uncontrolled environments and in the field.

Figure 2 illustrates the amplitude response prediction results. Good agreement is observed between observation (blue) and prediction (black) using the optimal parametric hydrodynamic database in conjunction with forward model VIVA. The amplitude is estimated well on average, especially for high flow velocities. Cases ”2010” and ”2040” in the amplitude response (Fig. 2) were ”cherry-picked” to demonstrate how the experimental results behave rather peculiarly at low flow velocities, since a non-symmetric response is observed in a symmetric problem. An unsymmetrical prediction is currently beyond our understanding of the flow physics and is a limitation of the current framework and forward model.

As is illustrated in Figure 3, the predicted frequency as a function of incoming flow velocity is estimated well across the full range of flow velocities, with a deviation of at most 15% observed at high flow speeds. At low flow velocities the prediction is very accurate while it starts to deviate as flow velocity increases.

It should be noted that there is significant evolution of the response as the database is refined during the optimization process. Figure 4 shows the amplitude response predicted using the nominal VIVA database (also used as initial condition for optimization) along with the amplitude response prediction of the converged optimal hydrodynamic database obtained after optimization. The two differ significantly both in terms of magnitude as well as in terms of mode number, with the optimized database predictions matching experiments more closely.

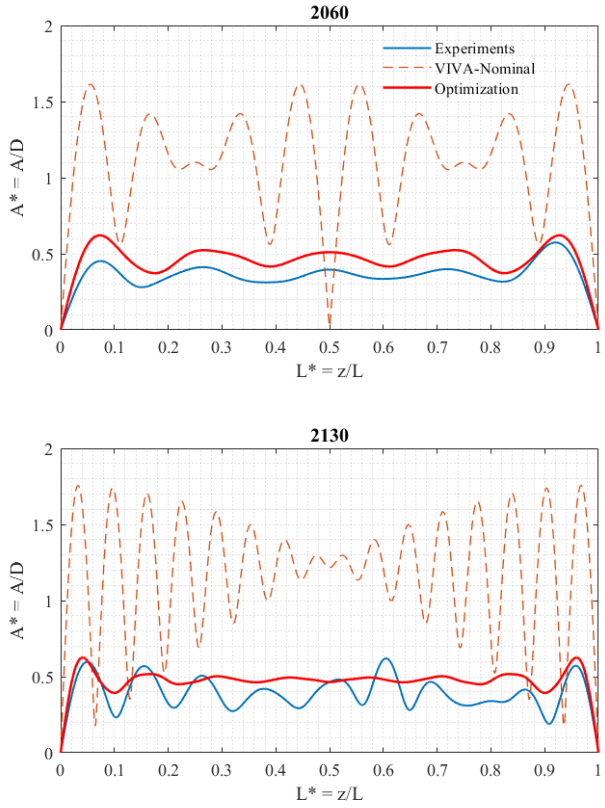

Fig. 4 Amplitude response evolution: Non-dimensional amplitude (y-axis) as a function of span (x-axis) for two flow velocities (each titled with an experiment number). Experimentally observed response (reconstructed) is shown as a blue solid line; prediction using the nominal VIVA database (also used as initial condition) is shown as an orange dashed line, while the prediction made using the converged optimal parametric hydrodynamic database is shown as a red solid line.

As Figure 4 illustrates, the amplitude responses evolve drastically as the database is refined during training. Predictions using the initial condition overestimate the amplitude by more than 50% on average and over-predict the mode number. The predictions using the converged optimal hydrodynamic database are superior to those of the initial condition in terms of predicting the vibration amplitude as well as in terms of capturing the mode number. It should be noted that the mode number for high flow velocities is harder to infer from experimental results as a structural response of travelling waves might appear as a high mode number; for some cases (for example case 2060 shown in Figure 4) both the amplitude and mode number are significantly better predicted using the optimal hydrodynamic database.

A closing remark is that extracting a hydrodynamic database takes approximately 5-10 hours, while each individual prediction (of amplitude and frequency response for a single flow velocity) takes less than 5 seconds. While the results are not perfect, this low fidelity model is able to make predictions comparable (and perhaps favorable after the

optimization) to much higher fidelity models of greater complexity and computational cost making this a competent candidate for multi-fidelity modelling and rough estimates of risers' structural responses.

CONCLUSION

A nineteen dimensional parametric framework has been used, which in conjunction with a forward VIV predictive model, such as VIVA (Triantafyllou *et al.*, 1999, Zheng *et al.*, 2011), may be used to extract hydrodynamic coefficient databases from data, a task which used to be intractable given the number of experiments required via rigid-cylinder forced vibrations.

The capability of the framework to infer databases has been demonstrated for uniform flexible cylinders in uniform flow using limited strain measurements. An appropriate physics-informed initialization of the optimization has also been determined.

The significant improvement of forward model predictions after the hydrodynamic coefficient database optimization, suggests that the underlying physics may be encoded in the inferred database, providing ample opportunity for further exploration. An easily identified research direction remains physically interpreting the acquired hydrodynamic coefficient databases and correlating features with physical observations. Furthermore, investigating the uniqueness and robustness of the optimization method are questions to be addressed in future research.

ACKNOWLEDGEMENTS

The authors would like to gratefully acknowledge support from the DigiMaR Consortium.

REFERENCES

Baek, H., and Karniadakis, G. E. (2009). Suppressing vortex-induced vibrations via passive means. Journal of Fluids and Structures, 25(5), 848-866.

Bearman, P. W. (2011). Circular cylinder wakes and vortex-induced vibrations. Journal of Fluids and Structures, 27(5-6), 648-658.

Bernitsas, M. M., and Raghavan, K. (2008, January). Reduction/suppression of VIV of circular cylinders through roughness distribution at 8× 103¡ Re¡ 1.5× 105. In International Conference on Offshore Mechanics and Arctic Engineering (Vol. 48227, pp. 1001-1005).

Bernitsas, M. M., Ofuegbe, J., Chen, J. U., and Sun, H. (2019, June). Eigen-solution for flow induced oscillations (viv and galloping) revealed at the fluid-structure interface. In International Conference on Offshore Mechanics and Arctic Engineering (Vol. 58776, p. V002T08A063). American Society of Mechanical Engineers. 352–365.

Braaten, H., and Lie, H., (2004), NDP riser high mode VIV tests main report.

Evangelinos, C., Lucor, D., and Karniadakis, G. E. (2000). DNS-derived force distribution on flexible cylinders subject to vortex-induced vibration. Journal of fluids and structures, 14(3), 429-440.

Fan, D., and Triantafyllou, M. S. (2017, June). Vortex induced vibration of riser with low span to diameter ratio buoyancy modules. In The 27th International Ocean and Polar Engineering Conference. OnePetro.

Fan, D., Wang, Z., Triantafyllou, M. S., and Karniadakis, G. E. (2019). Mapping the properties of the vortex-induced vibrations of flexible cylinders in uniform oncoming flow. Journal of Fluid Mechanics, 881, 815-858.

Fan, D., Wu, B., Bachina, D., and Triantafyllou, M. S. (2019). Vortex-induced vibration of a piggyback pipeline half buried in the seabed. Journal of Sound and Vibration, 449, 182-195.

Fan, D., Jodin, G., Consi, T. R., Bonfiglio, L., Ma, Y., Keyes, L. R., ... and Triantafyllou, M. S. (2019). A robotic intelligent towing tank for learning complex fluid-structure dynamics. Science Robotics, 4(36), eaay5063.

Gopalkrishnan, R. (1993). Vortex-induced forces on oscillating bluff cylinders. Woods Hole Oceanographic Institution MA.

Govardhan, R., and Williamson, C. H. K. (2002). Resonance forever: existence of a critical mass and an infinite regime of resonance in vortex-induced vibration. Journal of Fluid Mechanics, 473, 147-166.

Han, Q., Ma, Y., Xu, W., Fan, D., and Wang, E. (2018). Hydrodynamic characteristics of an inclined slender flexible cylinder subjected to vortex-induced vibration. International Journal of Mechanical Sciences, 148, 352-365.

Hover, F. S., Tvedt, H., and Triantafyllou, M. S. (2001). Vortex-induced vibrations of a cylinder with tripping wires. Journal of Fluid Mechanics, 448, 175-195.

Larsen, C. M. and Vikestad, K. and Yttervik, R. and Passano, E. and Baarholm, G. S. (2001). VIVANA theory manual. Marintek, Trondheim, Norway

Park, H., Kumar, R. A., and Bernitsas, M. M. (2016). Suppression of vortex-induced vibrations of rigid circular cylinder on springs by localized surface roughness at $3 \times 10^4 < Re < 1.2 \times 10^5$. Ocean Engineering, 111, 218-233.

Raghavan, K., and Bernitsas, M. M. (2011). Experimental investigation of Reynolds number effect on vortex induced vibration of rigid circular cylinder on elastic supports. Ocean Engineering, 38(5-6), 719-731.

Roveri, F. E., and Vandiver, J. K. (2001). SlenderEx: using SHEAR7 for assessment of fatigue damage caused by current induced vibrations. In Proceedings of the 20th International Conference on Offshore Mechanics and Arctic Engineering (pp. 3-8)..

Rudy, S., Fan, D., Ferrandis, J. D. A., Sapsis, T., and Triantafyllou, M. S. (2021, June). Learning optimal parametric hydrodynamic database for vortex-induced crossflow vibration prediction of both freely-mounted rigid and flexible cylinders. In The 31st International Ocean and Polar Engineering Conference. OnePetro.

Sarpkaya, T. (1978). Fluid forces on oscillating cylinders. Journal of the Waterway, Port, Coastal and Ocean Division, 104(3), 275-290.

Sarpkaya, T. (1995). Hydrodynamic damping, flow-induced oscillations, and biharmonic response. Journal of offshore Mechanics and Arctic engineering, 117(4).

Triantafyllou, M., Triantafyllou, G., Tein, Y. S., and Ambrose, B. D. (1999, May). Pragmatic riser VIV analysis. In Offshore technology conference. OnePetro.

Wang, X. Q., So, R. M. C., and Chan, K. T. (2003). A non-linear fluid force model for vortex-induced vibration of an elastic cylinder. Journal of Sound and Vibration, 260(2), 287-305.

Wang, J. S., Fan, D., and Lin, K. (2020). A review on flow-induced vibration of offshore circular cylinders. Journal of Hydrodynamics, 32(3), 415-440.

Wang, Z., Fan, D., and Triantafyllou, M. S. (2021). Illuminating the complex role of the added mass during vortex induced vibration. Physics of Fluids, 33(8), 085120.

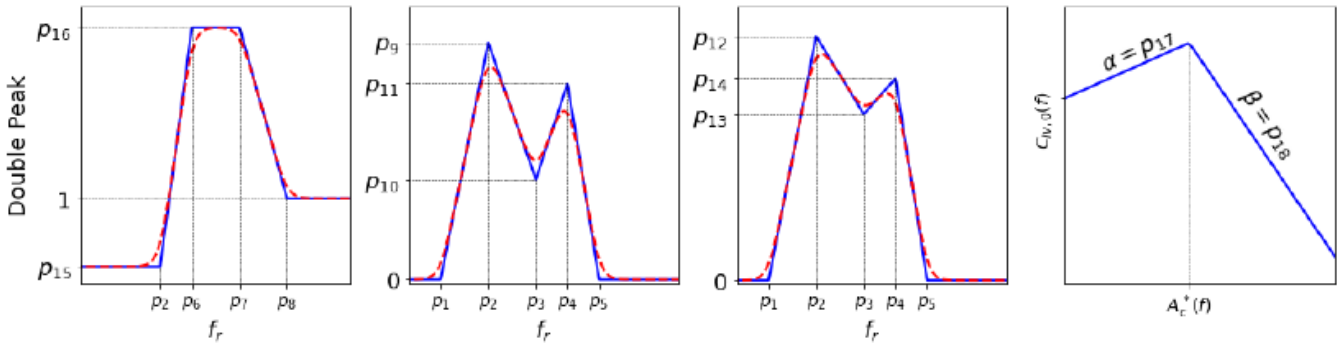

Fig. 5 Choice of Parametrization

Wang, Z., Fan, D., Triantafyllou, M. S., and Karniadakis, G. E. (2021). A large-eddy simulation study on the similarity between free vibrations of a flexible cylinder and forced vibrations of a rigid cylinder. Journal of Fluids and Structures, 101, 103223.

Williamson, C. H. (1996). Vortex dynamics in the cylinder wake. Annual review of fluid mechanics, 28(1), 477-539.

Williamson, C. H., and Govardhan, R. (2004). Vortex-induced vibrations. Annu. Rev. Fluid Mech., 36, 413-455.

Williamson, C. H. K., and Govardhan, R. (2008). A brief review of recent results in vortex-induced vibrations. Journal of Wind engineering and industrial Aerodynamics, 96(6-7), 713-735.

Wu, B., Le Garrec, J., Fan, D., and Triantafyllou, M. S. (2017, June). Kill line model cross flow inline coupled vortex-induced vibration. In International Conference on Offshore Mechanics and Arctic Engineering (Vol. 57649, p. V002T08A010). American Society of Mechanical Engineers.

Wu, X., Ge, F., and Hong, Y. (2012). A review of recent studies on vortex-induced vibrations of long slender cylinders. Journal of Fluids and Structures, 28, 292-308.

Wu, W., Bernitsas, M. M., and Maki, K. (2014). RANS simulation versus experiments of flow induced motion of circular cylinder with passive turbulence control at 35,000¡ Re¡ 130,000. Journal of Offshore Mechanics and Arctic Engineering, 136(4).

Xu, Y., Fu, S., Chen, Y., Zhong, Q., and Fan, D. (2013). Experimental investigation on vortex induced forces of oscillating cylinder at high Reynolds number. Ocean Systems Engineering, 3(3), 167-180.

Zheng, H., Price, R., Modarres-Sadeghi, Y., Triantafyllou, G. S., Triantafyllou, M. S. (2011, January). Vortex-induced vibration analysis (VIVA) based on hydrodynamic databases. In International Conference on Offshore Mechanics and Arctic Engineering (Vol. 44397, pp. 657-663).

APPENDIX I: HYDRODYNAMIC PARAMETRIZATION

The mathematical formulation of the parametric model is as follows. C_{my} is assumed to be a function of f_r, the true reduced frequency and the C_{lv} is assumed to be a function of both f_r and A^*, the non-dimensional amplitude. The quantities f_r an A^* are defined as follows:

$$f_r = \frac{f}{U \cdot D} \quad A^* = \frac{A}{D} \tag{3}$$

where f is the vibration frequency, U is the magnitude of incoming flow velocity, D is the riser's diameter, and A is the vibration amplitude. Before proceeding to the coefficient formulation, the softplus function should be first defined:

$$sf(x, \boldsymbol{p}) = p_{19} \cdot \ln\left(1 + \exp\frac{x}{p_{19}}\right) \tag{4}$$

where p_{19} serves as a scaling constant. Then, the C_{my} curve may be parametrized by Equation 5 as follows:

$$\begin{aligned}\hat{C}_{my}(f_r, \boldsymbol{p}) = p_{15} &+ \frac{p_{16} - p_{15}}{p_7 - p_2}[sf(f_r - p_2) - sf(f_r - p_7)] \\ &+ \frac{1 - p_{16}}{p_8 - p_7}[sf(f_r - p_7) - sf(f_r - p_8)]\end{aligned} \tag{5}$$

where $\hat{C}_{my}(f_r, \boldsymbol{p})$ is the parametric form of the C_{my} curve. The C_{lv_0} may be represented parametrically as shown in Equation 6.

$$\begin{aligned}\hat{C}_{lv,0}(f_r, \boldsymbol{p}) = &\frac{p_9}{p_2 - p_1}[sf(f_r - p_1) - sf(f_r - p_2)] \\ &+ \frac{p_{10} - p_9}{p_3 - p_2}[sf(f_r - p_2) - sf(f_r - p_3)] \\ &+ \frac{p_{11} - p_{10}}{p_4 - p_3}[sf(f_r - p_3) - sf(f_r - p_4)] \\ &+ \frac{-p_{11}}{p_5 - p_4}[sf(f_r - p_4) - sf(f_r - p_5)]\end{aligned} \tag{6}$$

where $\hat{C}_{lv,0}(f_r, \boldsymbol{p})$ is the parametric form of the $C_{lv,0}$ curve. Accordingly, the A_c^* curve may be represented as in Equation 7.

$$\begin{aligned}\hat{A}_c^*(f_r, \boldsymbol{p}) = &\frac{p_{12}}{p_2 - p_1}[sf(f_r - p_1) - sf(f_r - p_2)] \\ &+ \frac{p_{13} - p_{12}}{p_3 - p_2}[sf(f_r - p_2) - sf(f_r - p_3)] \\ &+ \frac{p_{14} - p_{13}}{p_4 - p_3}[sf(f_r - p_3) - sf(f_r - p_4)] \\ &+ \frac{-p_{13}}{p_5 - p_4}[sf(f_r - p_4) - sf(f_r - p_5)]\end{aligned} \tag{7}$$

where $\hat{A}_c^*(f_r, \boldsymbol{p})$ is the parametric form of the non-dimensional critical amplitude A_c^*. Finally, the value of the lift coefficient, C_{lv} may be calculated according to Equation 8.

$$C_{lv}(A^*, \boldsymbol{p}) = \begin{cases} \hat{C}_{lv,0} + p_{17} \cdot A^* & if A^* \le A_c^* \\ \hat{C}_{lv,0} + p_{17} \cdot \hat{A}_c^* - p_{18} \cdot (A^* - \hat{A}_c^*) & if A^* > A_c^* \end{cases} \quad (8)$$

The complete model of the parametric hydrodynamic coefficient database may be represented using 4 plots, one for each parametrized curve, i.e. C_{my}, C_{lv_0}, A_c^*, and C_{lv}, as shown in Figure 5 (in that order from left to right).

As Figure 5 illustrates, the model essentially parametrized the curves as smoothed piecewise linear functions and provides some flexibility in terms of magnitudes and transition points between linear sections. It should be noted that there exist shared parameters between the curves.

APPENDIX II: AMPLITUDE PREDICTION RESULTS

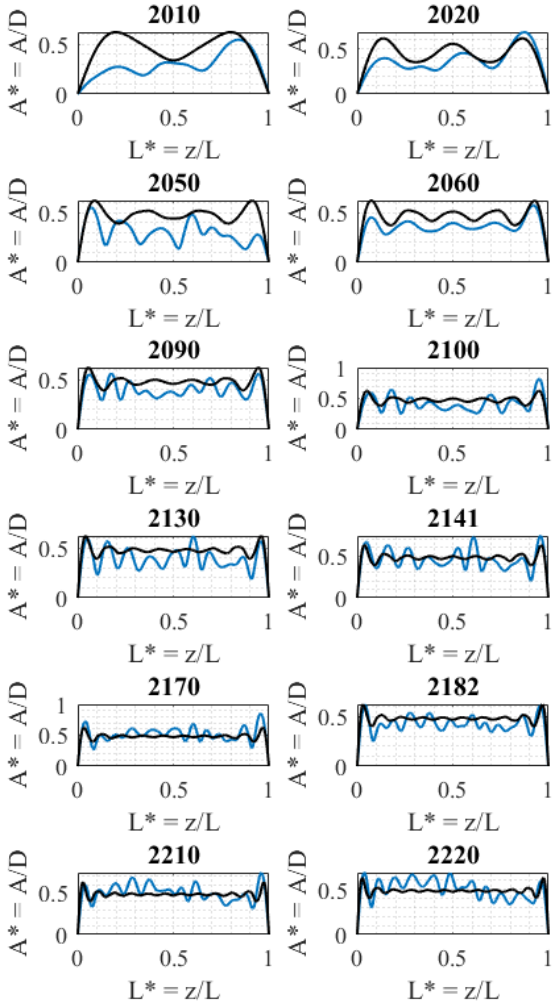

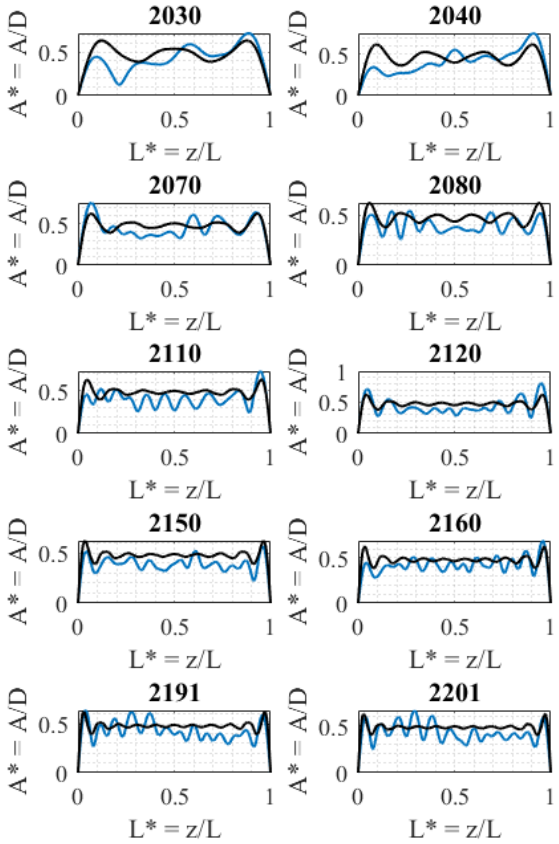

Fig. 6 Amplitude Prediction, complete set. Experiments (blue) and predictions (black).